Simulation of Quench Behavior in CS LTS Magnets for Next-Generation Compact Fusion Devices with Alternating Operation

Yu Chen, Yanlan Hu, Yezheng Xiao , Qing Yan, Longgui Zheng, Xinxin Zhu, Qicai Ni

Abstract—In the next generation of compact fusion devices, the central solenoid (CS) coil needs to provide a large alternating current and a magnetic field change rate of up to 7 T/s to achieve plasma breakdown, configuration formation and control. This alternating operation mode significantly affects the stability of the superconducting magnet. In order to protect the safety of superconducting magnets under alternating operation and provide a theoretical basis for setting the voltage threshold and time threshold of the quench protection system, it is necessary to understand the quench propagation characteristics of the CS coil cryogenic magnet under alternating current. this paper constructs an electromagnetic-thermal coupled numerical simulation model based on the THEA program. Thermal disturbances are applied in the three stages of current ramp-down, ramp-up and steadystate, and the minimum quench energy (MQE) and quench propagation behavior of each stage are compared. The results show that compared with the steady-state stage, the MQE in the ramp-up stage decreased by 14.11%, while the MQE in the rampdown stage increased by 21.58%. In terms of propagation rate, the voltage propagation rate and normal zone propagation velocity (NZPV) in the ramp-up stage were the highest, increasing by 31.4% and 16.7% respectively, while the ramp-down stage was the slowest, decreasing by 78.4% and 40.8% respectively. However, in the early stage of thermal disturbance application, due to the combined effects of current change and thermal disturbance power, the quench propagation in the current steady-state stage is the fastest, followed by the current ramp-down stage, and the current ramp-up stage is the slowest.

Index Terms—Alternating Current, Quench Propagation, Quench Simulation, THEA.

I. INTRODUCTION

he central solenoid magnet system of the next generation compact fusion energy experimental device is mainly used to determine and control the configuration of the plasma and to establish and maintain the plasma current within a certain time scale. The system consists of six central solenoid coils, each of which is divided into two submodules. Among them, the high field side (HF \leq 19.09 T) is

This work was supported in part by Comprehensive Research Facility for Fusion Technology Program of China under Contract No.2018-000052-73-01-001228, and in part by Research on Performance Improvement and Key Technology of Quench Detection System of EAST Device of China under E05F0K153Z1. (Corresponding author: Yanlan Hu)

Yu Chen is with the Institute of Plasma Physics, Hefei Institutes of Physical Science, Chinese Academy of Sciences, Hefei 230031, China, and also with University of Science and Technology of China, Hefei 230026, China (e-mail: yu.chen1@ipp.ac.cn).

wound with YBCO CICC high temperature superconductor (HTS submodule) [1],[2], while the low field side (LF \leq 12.69 T) is wound with Nb₃Sn CICC low temperature superconductor (LTS submodule) [3], as shown in the **Fig. 1**.

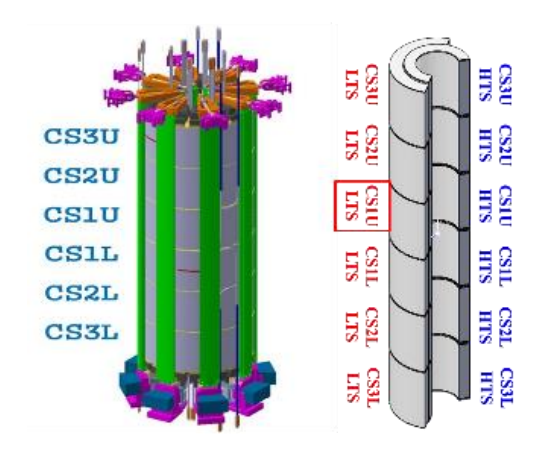


Fig. 1. The CS coil structure, the CS1U-LTS coil is the subject of this study.

The CS coil plays a key role in plasma initiation, shape formation, and equilibrium control. It must be capable of delivering large alternating currents and extremely rapid magnetic field ramp rates-up to 7 T/s [4]. Under such operational conditions, the alternating stability superconducting magnets is significantly challenged. On one hand, shielding current effects may arise in the superconducting tapes during excitation, affecting the uniformity and stability of the magnetic field. On the other hand, the high current ramp rates during fast charging and discharging can induce substantial thermal accumulation [5]. If the superconducting coil contains manufacturing defects—such as impurities, cracks, or micro-voids—these may act as local hot spots, leading to significant local temperature rise. This can cause premature quenching of the superconducting material, resulting in the formation of localized resistive zones.

Yanlan Hu is with the Institute of Plasma Physics, Hefei Institutes of Physical Science, Chinese Academy of Sciences, Hefei 230031, China (e-mail: yanlanghun@ipp.ac.cn).

Yezheng Xiao, Qing Yan, Longgui Zheng, Xinxin Zhu and Qicai Ni are with the Institute of Plasma Physics, Hefei Institutes of Physical Science, Chinese Academy of Sciences, Hefei 230031, China.

In simulation studies of the ITER CS coil by L. Cavallucci et al. and the CFETR CSMC coil by Aiguo Sang et al., the operating conditions were assumed to be stable current and an unchanging background magnetic field, in order to investigate quench propagation characteristics [6],[7]. However, in next-generation fusion experimental devices, all coils are required to generate rapidly varying magnetic fields. Specifically, the background magnetic field of the CS coil exhibits strong temporal variation, and its operating current is inherently alternating. However, in next-generation fusion experimental devices, the coils are expected to operate under rapidly changing magnetic fields. Specifically, the CS coil experiences a strongly time-varying background field and carries an alternating current.

To investigate the quench propagation behavior of superconducting magnets under transient conditions, the CS1U-LTS module in the CS coil located in the central area with large current and magnetic field changes was selected as the research object. Electromagnetic field simulations of the entire superconducting magnet system are first performed to obtain the background magnetic field variation experienced by the CS1U-LTS module under rapidly alternating conditions. This time-varying field is then used as the background field in the subsequent quench simulations.

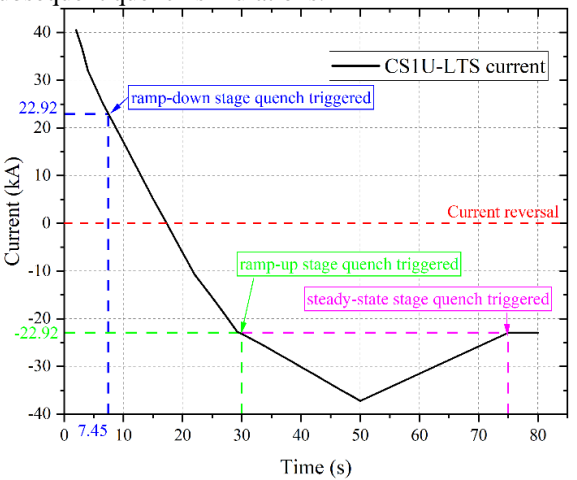


Fig. 2. Current waveform and trigger quench position at each stage.

An extended version of the CryoSoft code THEA is employed to develop a transient electromagnetic—thermal coupled model of the CS1U-LTS coil for quench simulation. The operating current of the CS1U-LTS module includes a ramp-down stage, a ramp-up stage, and a steady-state stage (i.e., the final moment of the waveform). Thermal disturbances are applied at each stage to analyze the variation in quench propagation characteristics under alternating current conditions. The locations of thermal disturbance applied at each stage are shown in the **Fig. 2**.

II. MAGNETIC FIELD ANALYSIS

A. Parameters

Since the current in the TF coils varies slowly—or remains

nearly constant—their mutual inductance with the CS coil is negligible, and their dynamic influence on the CS coil can be ignored. To reduce computational complexity, the effect of the TF coils is therefore excluded when analyzing the background magnetic field variation of the CS1U-LTS module.

The superconducting magnet system of the next-generation fusion experimental device primarily consists of CS coils, PF coils, and CC coils. The composition of the CS coils has been described in Chapter 1. The PF system includes seven coils (PF1–PF7), while the CC system consists of eight coils symmetrically arranged around the PF coils. The detailed configuration is illustrated in the **Fig. 3**. The mutual inductance between CS1U-LTS and each coil is in the TABLE I. The current waveform applied to each coil is shown in the **Fig. 4**. Based on the information provided above, the magnetic field changes of the CS1U-LTS module can be calculated in the finite element analysis software.

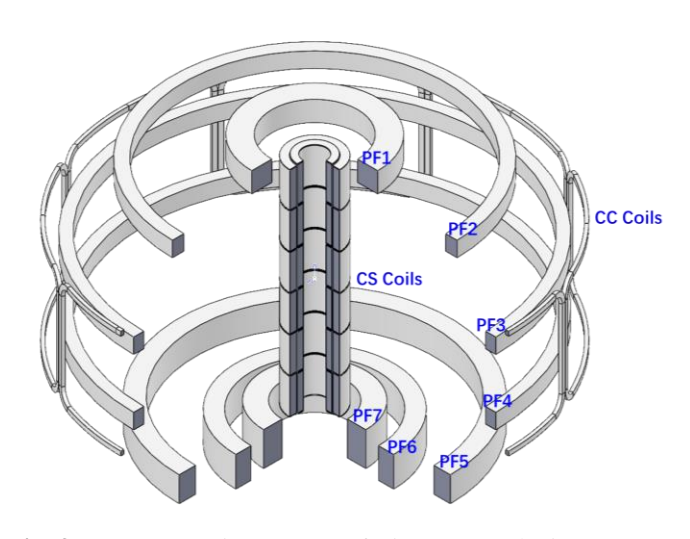


Fig. 3. Next generation compact fusion energy device magnet system (excluding TF coil).

TABLE I

MUTUAL INDUCTANCE BETWEEN CS1U-LTS AND EACH

COIL, UNIT: MH						
LTS	[mU]	HTS	ГтП	PF	[m[]]	
Coil	[mH]	Coil	[mH]	Coil	[mH]	
CS3U	23.9	CS3U	6.45	PF1	1.4	
CS2U	3.80	CS2U	0.91	PF2	2.56	
CS1U	99.8	CS1U	24.7	PF3	4.20	
CS1L	1.17	CS1L	0.27	PF4	5.65	
CS2L	23.9	CS2L	5.94	PF5	14.9	
CS3L	0.5	CS3L	0.11	PF6	13.5	
				PF7	10.1	

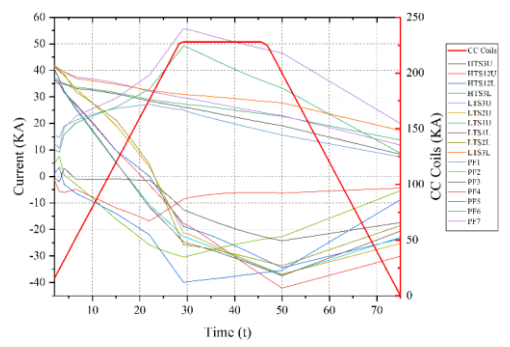


Fig. 4. Current waveform of each coil.

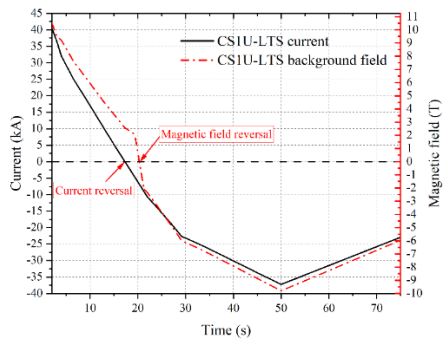


Fig. 5. Waveforms of current and magnetic field.

B. Magnetic Field Results

Based on the predefined current profiles of each coil, a magnetic field simulation of the system was performed. Considering the extreme case, the magnetic field evolution at the point of maximum field strength was used as a representative profile for the entire CS1U-LTS module (as shown in the **Fig. 5**).

Simulation results show that although the magnetic field strength of the CS1U-LTS module is influenced by the coupling of multiple coils, its variation trend remains largely consistent with its own operating current, indicating that the dynamic response of the magnetic field is primarily driven by the coil's own current. The maximum magnetic field strength reaches approximately 10.5 T, occurring near the current peak, and decreases during the current ramp-down phase—further confirming the synchronization between current and magnetic field variations.

To simulate a more realistic operational condition, the dynamic magnetic field profile obtained in this chapter is used as an input for the subsequent quench simulations, allowing for the investigation of quench propagation characteristics under simultaneously alternating current and magnetic field conditions.

III. QUENCH SIMULATION

A. Numerics

The electromagnetic-thermal coupling numerical model of the CS1U-LTS coil under alternating current conditions has been developed using the CryoSoft code THEA. A detailed description of the THEA model can be found in [8]. To more accurately simulate the response characteristics of superconducting magnets under complex operating conditions, key simulation parameters are summarized in Table II. These parameters include the geometric configuration, material properties, and operating conditions of the magnet, ensuring the reliability and comparability of the simulation results. The current waveform shown in the **Fig. 2** was applied in the simulation, with quench triggers introduced at the ramp-up, ramp-down, and steady-state stages. This approach enables a comprehensive analysis of the quench evolution under different dynamic conditions.

To ensure the comparability of simulation results across all stages, all quench simulations were conducted under identical operating conditions. The selected CS1U-LTS module adopts an 8-in/8-out cooling configuration, with each individual flow channel having an approximate length of 100 m. The detailed cooling structure is illustrated in the Fig. 6. According to the electromagnetic field simulation results presented in Chapter 2, the maximum magnetic field occurs within the central flow channel. Therefore, this central channel is chosen as the target region for quench simulation. The helium mass flow rate is set to 6 g/s, with an inlet pressure of 5 bar and a pressure drop of 0.25 bar. The magnet is assumed to be in an adiabatic environment, thereby eliminating the influence of external heat exchange. This setup effectively isolates and highlights the influence of current variations and dynamic magnetic field behavior on quench propagation.

TABLE II
QUENCH SIMULATION PARAMETERS

Conductor Type	CS1U-LTS
RRR (Residual Resistivity Ratio)	100
Central Hole Hydraulic Diameter [m]	6.0e-3
Bundle Hydraulic Diameter [m]	0.82e-3
Wetted Perimeter – bundle [m]	1.39
Wetted Perimeter - jacket [m]	9.1e-2
Helium Hole Area [m²]	28.3e-6
Helium Bundle Area [m²]	98.2e-6
SC Cross-Sectional [m²]	1.43e-4
Copper Cross-Sectional [m²]	1.47e-4
Jacket Cross-Sectional [m ²]	5.15e-4
Void fraction (Bundle)	~26%

B. Quench Detection and Current

The current waveform used in this simulation corresponds to the predefined operating profile of the next-generation fusion device. To enable a comparative analysis of quench propagation characteristics at different stages, it is essential to maintain a consistent operating current across all quench trigger scenarios. In this study, a current value of 22.9 kA, corresponding to the steady-state stage, is selected as the quench initiation point. Quench simulations are subsequently conducted during the current ramp-down stage, the ramp-up stage, and the steady-state stage. The current rates differ among these stages: 2.3 kA/s during the ramp-down phase, and 0.7 kA/s during the ramp-up

phase.

To effectively monitor and initiate the quench process, the quench detection and protection parameters are configured as listed in Table III.

When the quench trigger is detected, the current is discharged in an exponential form (please note that AC losses are not considered in the simulation stage), and the discharge equation is as (1):

$$I = I_{op} e^{-t/\tau} \tag{1}$$

Where $\tau = L/R = 0.814$ is the characteristic time constant, which determines the decay rate of the current, I_{op} is the initial current temperature at the time of triggering the quench.

TABLE III
QUENCH DETECTION PARAMETERS

QUENCH BETECHON I AKAMETEKS			
Voltage threshold [mV]	100		
Time threshold [s]	1		
Protection switch delay time [s]	0.5		
Bleeder resistor $[\Omega]$	0.1325		
CS1U-LTS inductance [H]	0.10788		

C. Thermal Disturbance

The quench of the CS1U-LTS coil is triggered by applying a local thermal disturbance in the form of a thermal pulse with a length of 1 cm and a duration of 1 s. The same type of disturbance is applied during the current ramp-down phase, ramp-up phase, and steady-state phase to ensure consistency. By gradually increasing the power of the thermal disturbance, the precise MQE for each phase is obtained [9]. To eliminate or reduce the influence of pressure and temperature variations of the helium source at both ends of the coil, the thermal disturbance is applied at the center of the flow channel (approximately 50 m).

- The disturbance is applied at 7.45 s during the current ramp-down stage, when the operating current is 22.9 kA with a rate of 2.37 kA/s.
- 2) The disturbance is applied at 30.0 s during the current ramp-up stage, when the operating current is -22.9 kA with a rate of 0.7 kA/s.
- 3) The disturbance is applied at 75.0 s during the steady-state stage, when the operating current is -22.9 kA.

Note: The positive and negative signs of the current represent opposite directions only and do not affect the quench behavior, as shown in the **Fig. 2**.

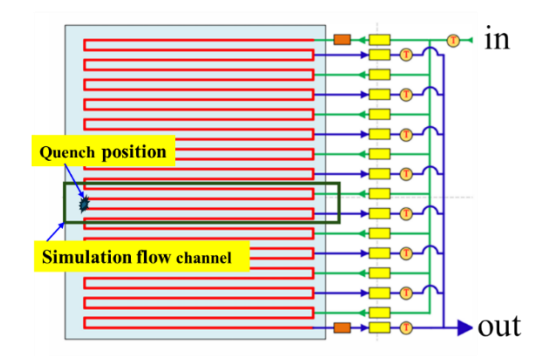


Fig. 6. CS1U-LTS cooling circuit and quench position.

IV. RESULTS AND DISCUSSION

A. MQE

During the current descending, rising, and steady-state stages, the power of the thermal disturbance is gradually increased until the CS1U-LTS module is triggered to quench. The corresponding temperature evolution is shown in the **Fig. 7**. From the figure, the minimum heating power required to trigger a quench at each stage can be clearly observed. The corresponding Minimum Quench Energy (MQE) is calculated using the equation (2), Superconducting magnets have been extensively studied [10].

$$Q_{MQE} = \frac{Q \cdot \Delta L \cdot \Delta t}{(A_{SC} + A_{Cu}) \Delta L \times 10000}$$
 (2)

Where Q_{MQE} represents the minimum quench energy, Q is the disturbance power, ΔL is the disturbance length, Δt is the thermal disturbance duration, A_{sc} is the cross-sectional area of the superconducting strands, A_{Cu} is the cross-sectional area of the copper in the conductor.

The calculated minimum quench energy at each stage is as TABLE IV:

TABLE IV MQE AT EACH STAGE

Different quench stages	$MQE [J/cm^3]$	Time span [s]
ramp-down stage	2.93	4.81
ramp-up stage	2.07	2.14
steady-state stage	2.41	2.67

From the TABLE IV, it can be observed that the MQE is highest during the ramp-down stage, being 21.58% greater than that in the steady-state stage. Conversely, the MQE is lowest during the ramp-up stage, showing a 14.11% reduction compared to the steady-state. This behavior is attributed to the fact that during the ramp-up stage, once the superconductor partially transitions out of the superconducting state, its current is in a state of increasing, increased Joule heating occurs. This leads to a reduction in the stability margin of the conductor, thereby lowering the required MQE.

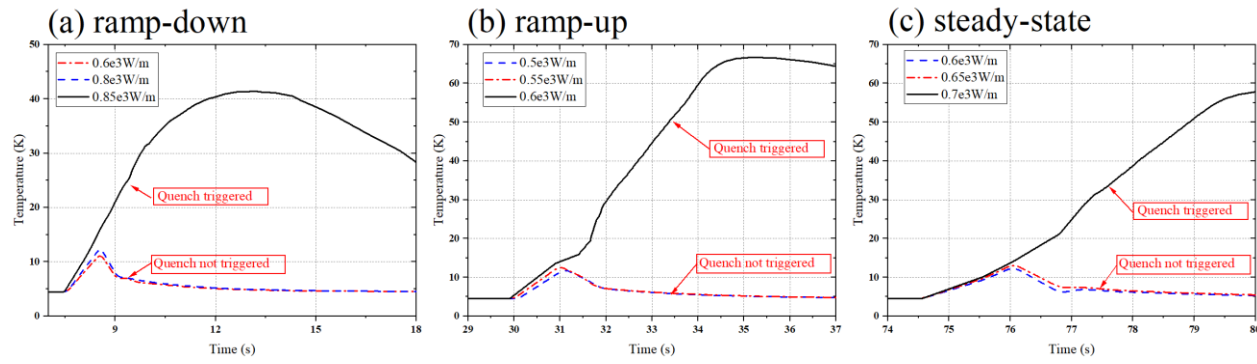


Fig. 7. Temperature curves at different disturbance powers in each stage.

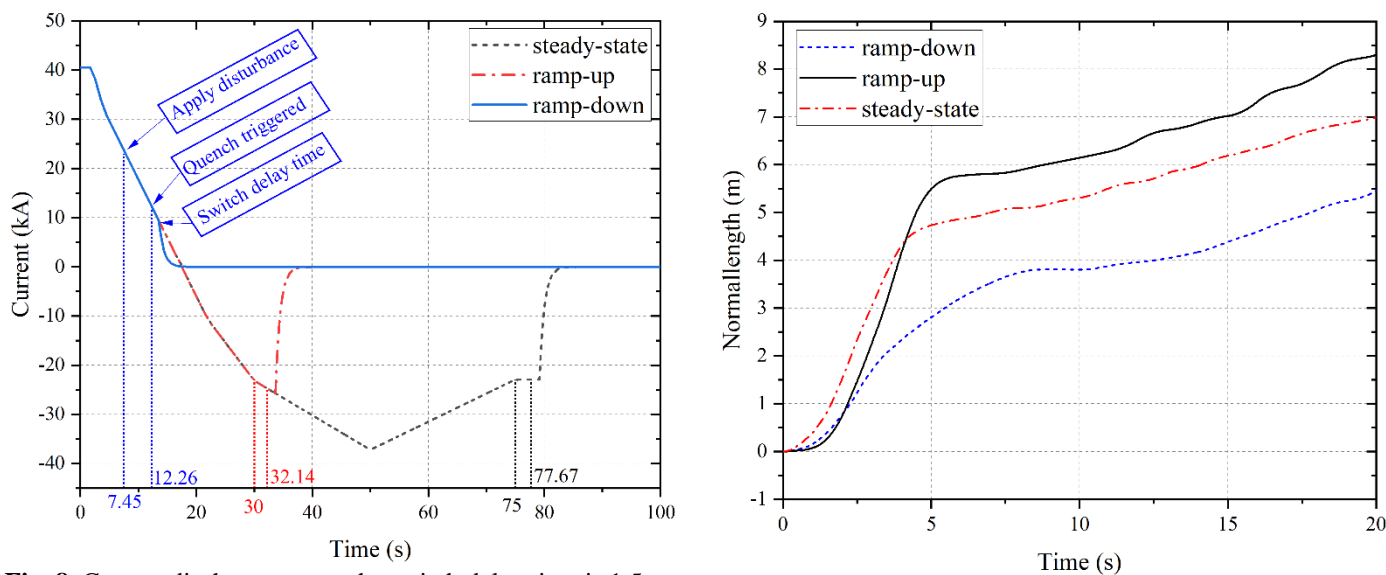


Fig. 8. Current discharge curve, the switch delay time is 1.5s.

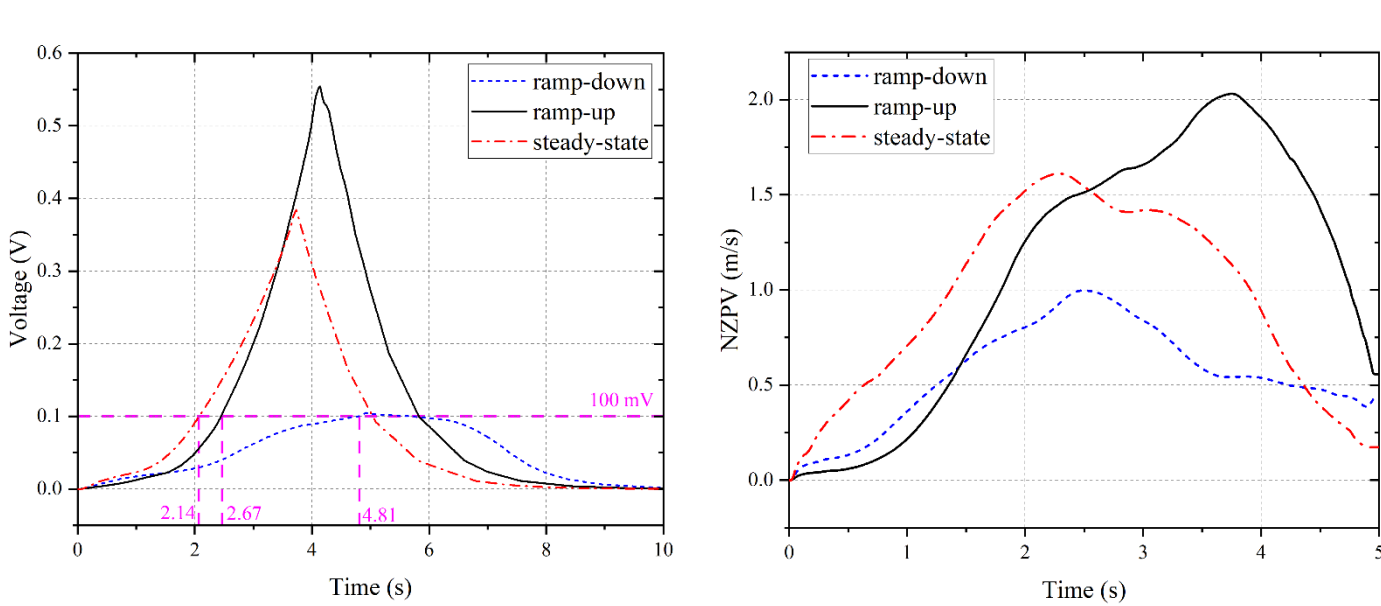


Fig. 9. Voltage propagation curves at each stage.

Fig. 11. Time evolution of the normal zone propagation velocity (NAPV).

Fig. 10. Normal zone propagation curves at each stage.

B. Current Discharge

As shown in the **Fig. 8**, the time span between the application of thermal disturbance and the onset of quench varies across different operating stages due to the differing current evolution that follows. The specific values are summarized in TABLE IV.

During the ramp-down stage, the time interval from the application of thermal disturbance to quench onset is 4.81 s, which is 2.14 s longer than that in the steady-state stage. This is because the working current in this stage decreases rapidly at a rate of 2.37 kA/s, requiring a longer time for the heat deposition to reach the MQE threshold.

In contrast, during the ramp-up stage, the time interval is 2.14 s, which is 0.53 s shorter than that in the steady-state stage. This is due to the increasing current at a rate of 0.7 kA/s, resulting in faster energy accumulation and reduced time to reach quench conditions.

These results indicate that under alternating current operation, the quench trigger time is stage-dependent. If a thermal disturbance occurs during the ramp-up phase, the quench detection time threshold should be appropriately reduced to ensure timely protection response.

C. Voltage and Normal Zone Propagation

Considering that quenching in the three stages does not occur simultaneously, this study uniformly selects data within the same time window starting from the onset of thermal disturbance to enable a fair comparison of voltage response and normal zone propagation behavior. The absolute values of voltage are used for each stage to facilitate numerical comparison.

As shown in the **Fig. 9**, the time at which the quench is triggered differs across the three operating stages. Using the point where the coil voltage reaches 100 mV as a reference, the voltage rise is fastest during the current ramp-up stage, followed by the steady-state stage, and slowest during the ramp-down stage. However, within the first second, the voltage propagation behaves slightly differently: the steady-state stage exhibits the fastest initial voltage increase, followed by ramp-down stage, and the slowest is in the ramp-up stage.

This behavior is primarily due to the variation in applied thermal disturbance power. During the first second, the thermal disturbance power in the ramp-down stage is significantly higher than in the ramp-up stage, resulting in a local "lead" in voltage response. However, because of the rapid current decay (2.37 kA/s), the additional heat input does not significantly exceed that in the steady-state stage, leading to an overall slower propagation rate.

As shown in the **Fig. 10**, the normal zone propagation behavior across the three stages exhibits a trend consistent with the voltage response. **Fig. 11** shows the change of NZPV more clearly. In the first 1.5 seconds, although the current is decreasing in the ramp-down stage and increasing in the ramp-up stage, the NZPV is still in the leading position in the ramp-down stage because the applied disturbance power is significantly greater than that in the ramp-up stage. In the steady-state stage, the NZPV is ahead of the deceleration stage

because the current is larger and the disturbance power is only slightly less than that in the ramp-down stage. Overall, the law shown by NZPV is still that the ramp-up stage is greater than the steady-state stage, and the steady-state stage is greater than the ramp-down stage.

The average propagation speed from the application of the thermal disturbance to the voltage peak, as well as the normal zone velocity and temperature rise rate within the first 5 seconds, are summarized in the TABLE V.

TABLE V
QUENCH PROPAGATION VELOCITY AT DIFFERENT
CURRENT STAGES

CURRENT STAGES					
stages	dV/dt	NZPV	Tmax	dT/dt	
	[V/s]	[m/s]	[K]	[K/s]	
ramp- down	0.022	0.559	41.32	8.26	
ramp- up	0.134	1.103	66.59	13.32	
steady- state	0.102	0.945	57.94	11.59	
	•		•	•	

The results indicate that, compared with the steady-state stage, triggering a quench during the ramp-up stage accelerates the propagation of both voltage and the normal zone. Specifically, under a current ramp-up rate of 0.7 kA/s, the voltage propagation speed increases by approximately 31.4%, and the normal zone propagation speed increases by about 16.7%. Conversely, during the ramp-down stage with a current decrease rate of 2.37 kA/s, the voltage propagation speed decreases by around 78.4%, and the normal zone propagation speed drops by approximately 40.8%. Based on the above analysis, a qualitative conclusion can be drawn: the propagation of voltage and the normal zone is accelerated during current ramp-up and decelerated during current ramp-down, with the degree of variation correlated to the rate of current change.

D. Maximum Temperature Rise

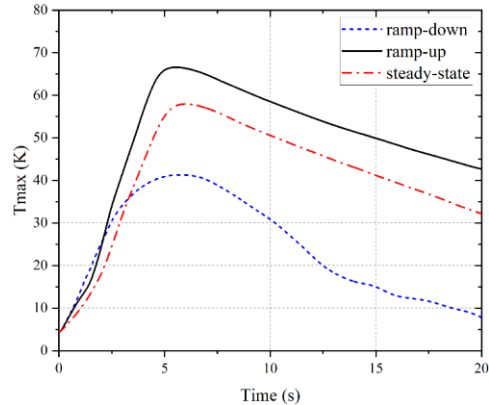


Fig. 12. Maximum temperature (Tmax) rise curve at each stage (hot spot temperature).

In the three quenching stages analyzed in this study, the thermal disturbance is triggered when the operating current reaches 22.9 kA. At this moment, the current is relatively low and the background magnetic field is comparatively weak, resulting in a moderate peak temperature rise in all cases—well

within the magnet design limit of 150 K, as shown in the **Fig.** 12. The hot spot temperatures for each stage are listed in the table above. Compared with the steady-state stage, the hot spot temperature during the ramp-up stage increases by 14.93%, while it decreases by 28.68% in the ramp-down stage.

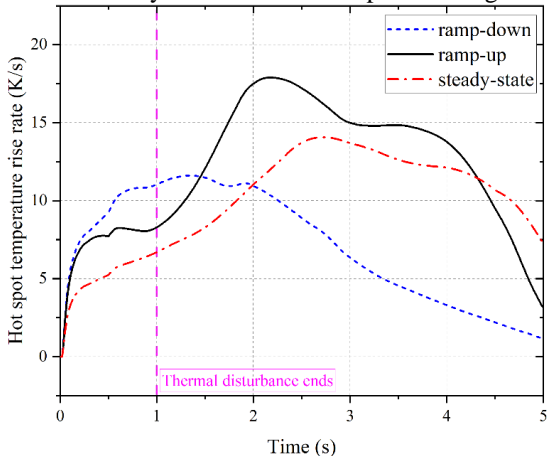


Fig. 13. Temperature rise rate of each stage changes with time.

The TABLE V also presents the average temperature rise rates during the first 5 seconds for each stage. Although the average rate is highest during the ramp-up stage, followed by the steady-state and then the ramp-down stage, the detailed evolution of temperature is more nuanced. As shown in the **Fig.** 13, within the initial 1.5 seconds, the ramp-down stage exhibits the highest temperature rise rate. This is because, despite the decreasing current, the MQE is largest in this stage, requiring a higher thermal disturbance power, which accelerates initial heating.

After approximately 4.2 seconds, the steady-state stage surpasses the ramp-up stage in temperature rise rate. This is attributed to the later quench trigger time in the steady-state stage, allowing for additional Joule heat accumulation over a short period.

V. CONCLUSION

In this paper, a numerical model of electromagnetic—thermal coupled quench behavior is developed for CS1U-LTS superconducting magnets in a next-generation compact fusion energy experimental device, under conditions of rapid current variation. This model is established by extending the THEA program. The study focuses on a detailed analysis of the differences in quench propagation characteristics when the quench is initiated during the ramp-down, ramp-up, and steady-state current stages.

The results show that, compared to the steady-state stage, the MQE required to initiate a quench is reduced by 14.11% during the ramp-up stage, while it increases by 21.58% during the ramp-down stage. In terms of propagation behavior, the ramp-up stage exhibits the highest voltage propagation rate and normal zone expansion speed, with respective increases of 31.4% and 16.7%. In contrast, the ramp-down stage presents the slowest propagation, with decreases of 78.4% and 40.8%, respectively. In view of the significant increase in voltage

propagation rate and NZPV during the ramp-up stage, the quench protection time threshold and voltage threshold used in alternating operation should be appropriately lowered. The specific threshold values can be determined based on simulation results and protection criteria.

Interestingly, in the early stage of thermal disturbance application, the response characteristics of each stage show different trends. Due to the significantly higher thermal disturbance power during the ramp-down stage compared to the ramp-up stage, a transient "leading" voltage response is observed at the initial time. However, because the current decay rate is relatively fast (2.37 kA/s), the thermal disturbance power does not increase substantially compared to the steady-state stage. As a result, the overall propagation rate during the ramp-down stage remains slower than that of the steady-state condition.

This study provides detailed information on the propagation of quench characteristics of CS1U-LTS under alternating operation, which can provide a reliable theoretical basis for the subsequent setting of quench protection system parameters.

ACKNOWLEDGMENT

We thank the staff members of the Experimental Advanced Superconducting Tokamak (https://cstr.cn/31130.02.EAST), for providing technical support and assistance in data collection and analysis.

REFERENCES

- [1] H. Jin et al., "Performance test of REBCO CICC sub-cables with 10 kA current under 20 T background field," Supercond. Sci. Technol., vol. 36, no. 12, p. 12LT01, Dec. 2023, doi: 10.1088/1361-6668/ad0473.
- [2] H. Liu et al., "Manufacturing and performance test of a 21.59 kA @77 K, self-field full-size REBCO-HFRC cable-in-conduit conductor," Fusion Engineering and Design, vol. 211, p. 114775, Feb. 2025, doi: 10.1016/j.fusengdes.2024.114775.
- [3] R. Riccioli, A. Torre, D. Durville, M. Breschi, and F. Lebon, "Mechanical Analysis of Full-Scale Nb3 Sn CICC Designs for Tokamaks," IEEE Trans. Appl. Supercond., vol. 32, no. 6, pp. 1–5, Sep. 2022, doi: 10.1109/TASC.2022.3156967.
- [4] H. Liu et al., "Experimental study on the critical current in highly flexible REBCO cables under copper tube compaction," Fusion Engineering and Design, vol. 209, p. 114707, Dec. 2024, doi: 10.1016/j.fusengdes.2024.114707.
- [5] W. Yi, Q. Zhang, Y. Zhao, K. Zhu, Y. Wang, and Z. Li, "Design and AC Loss Study of a High-Temperature Superconducting CS Model Magnet for Fusion Applications," J Supercond Nov Magn, vol. 38, no. 2, p. 98, Apr. 2025, doi: 10.1007/s10948-025-06934-7.
- [6] L. Cavallucci, F. Gauthier, M. Breschi, C. Hoa, P. Bauer, and A. Vostner, "Multiphysics Model of Quench for the ITER Central Solenoid," IEEE Trans. Appl. Supercond., vol. 33, no. 5, pp. 1–5, Aug. 2023, doi: 10.1109/TASC.2023.3244769.
- [7] A. Sang et al., "Quench Simulation of the CFETR Central Solenoid Model Coil," IEEE Trans. Appl. Supercond., vol. 34, no. 5, pp. 1–7, Aug. 2024, doi: 10.1109/TASC.2024.3390088.
- [8] L. Bottura, "Modelling stability in superconducting cables," Physica C: Superconductivity, vol. 310, no. 1–4, pp. 316–326, Dec. 1998, doi: 10.1016/S0921-4534(98)00482-1.
- [9] H. Liu et al., "Minimum quench energy analysis for Six-Around-One HTS cable-in-conduit conductor," Fusion Engineering and Design, vol. 211, p. 114779, Feb. 2025, doi: 10.1016/j.fusengdes.2024.114779.
- [10] M. N. Wilson, Superconducting Magnets. Oxford, U.K.: Oxford Univ. Press, 1983.